Synthesis of longitudinal coherence functions by spatial modulation of an extended light source: a new interpretation and experimental verifications

Wei Wang, Hirokazu Kozaki, Joseph Rosen, and Mitsuo Takeda

Giving a new physical interpretation to the principle of longitudinal coherence control, we propose an improved method for synthesizing a spatial coherence function along the longitudinal axis of light propagation. By controlling the irradiance of an extended quasi-monochromatic spatially incoherent source with a spatial light modulator, we generated a special optical field that exhibits high coherence selectively for a specific pair of points at specified locations along the axis of beam propagation. This function of longitudinal coherence control provides new possibilities for dispersion-free measurements in optical tomography and profilometry. A quantitative experimental proof of principle is presented.

OCIS codes: 120.3180, 030.1640, 120.6650, 070.2580, 120.2830, 120.3940.

1. Introduction

Optical coherence tomography[1–3] and low-coherence profilometry[4–7] have been studied extensively. They use the physical property of broadband light that high-contrast fringes can be observed only when the beams from the sample and the reference mirror have the same optical path lengths. In other words, they are based on the common basic principle in which the characteristic of longitudinal coherence plays a crucial role. Usually the term "longitudinal coherence" is identified with temporal coherence,[8] for which coherence between two points along the propagation axis is determined by the temporal spectrum of the radiating source. However, if one notes the analogies between temporal and spatial parameters that are found in many optical phenomena,[9] one may think of yet another scheme for controlling longitudinal coherence by changing the spatial (rather than the temporal) structure of the radiating source. McCutchen,[10] Biegen,[11] and Rosen and Yariv[12,13] have shown that the longitudinal coherence between two points along the propagation axis can be determined purely from the spatial structure of a quasi-monochromatic incoherent planar source. In analogy to the relation of the temporal coherence to the source spectrum by the Wiener–Khintchine theorem, the generalized Van Cittert–Zernike theorem[12,13] relates the longitudinal spatial coherence to the spatial structure of the extended source. More recently, Rosen and Takeda[14] proposed a new scheme for surface profilometry based on longitudinal spatial coherence. Whereas conventional coherence tomography and low-coherence profilometry use a spectrally broad (i.e., temporally incoherent) and spatially confined (i.e., spatially coherent) point source (e.g., a superluminescent diode), our technique uses a spectrally narrow (i.e., quasi-monochromatic and temporally coherent) and spatially extended (i.e., spatially incoherent) source. The use of the narrow-band source can be an advantage when the object or the medium through which the light propagates has strong dispersion or inhomogeneous spectral absorption. The system requires no optical elements (such as a dispersion-compensation glass plate in a white-light Michelson interferometer) for dispersion correction. If a highly absorbing object or medium has a low-absorbing spectral window, the use of the quasi-monochromatic source permits one to tune the spectrum to the low-absorbing spectral window. Conventional coherence tomography and low-

W. Wang is with the Department of Physics, University of Science and Technology of China, 230026, Hefei, Anhui, China. W. Wang, H. Kozaki, and M. Takeda (takeda@ice.uec.ac.jp) are with the Department of Information and Communication Engineering, The University of Electro-Communications, 1-5-1, Chofugaoka, Chofu, Tokyo 182-8585, Japan. J. Rosen is with the Department of Electrical and Computer Engineering, Ben-Gurion University of the Negev, P.O. Box 653, Beer-Sheva 84105, Israel.
Received 21 July 2001.
0003-6935/02/101962-10$15.00/0

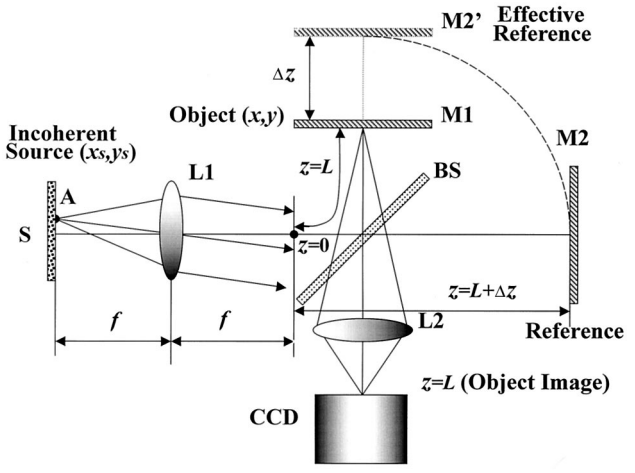

Fig. 1. Optical system for measuring the longitudinal complex degree of coherence. Abbreviations are defined in text.

coherence profilometry require mechanical movement of the reference mirror for the change in the optical path difference because their longitudinal (temporal) coherence function is invariable, as it is determined by the spectrum of the light source. The proposed technique needs no mechanism to change the optical path difference because the longitudinal (spatial) coherence function is varied with a spatial light modulator in such a manner that high-contrast fringes are observed at the desired optical path difference. In a space–time analogy,[9] our scheme for synthesizing spatial coherence is conceptually analogous to the synthesis of temporal coherence proposed by Hotate and Okugawa,[15] though the specific techniques used are completely different.

In this paper, first we present a new physical interpretation of the principle of longitudinal spatial coherence synthesis. Based on this new interpretation, we propose an improved technique for controlling longitudinal coherence and demonstrate its validity by experiments with quantitative data analysis. Finally, we discuss alignment, with particular emphasis on the influence of tilt on fringe visibility.

2. Principle

A. Description by Fourier Optics

Before giving a new physical interpretation of the principle of longitudinal coherence synthesis, we first review the basic principle in terms of Fourier optics along the lines of a paper by two of the present authors.[14]

A schematic diagram of the proposed system is illustrated in Fig. 1. A Michelson interferometer is illuminated by an extended quasi-monochromatic spatially incoherent light source (S) located at the front focal plane of lens L1. Light emitted from point A(x_s, y_s) of the source is collimated by lens L1 and is split into two beams by beam splitter BS. One beam is reflected from mirror M1, which serves as an object, and the other is reflected from mirror M2, which serves as a reference. Mirrors M1 and M2 are located at distances $z = L$ and $z = L + \Delta z$, respectively, from the rear focal plane of collimating lens L1. The interference fringes generated on the CCD image sensor are the result of combining the images of the two optical field distributions; one is the optical field distribution at object mirror M1, and the other is the optical field distribution created at the corresponding location in the reference arm by reference mirror M2. Both images are obtained by imaging lens L2, and the CCD image sensor records the intensity of these fringes.

The point source, with complex amplitude $u_s(x_s, y_s)$ at A, creates behind lens L1 a field distribution

$$u(x, y, z) = \frac{u_s(x_s, y_s)}{j\lambda f} \exp\left[j \frac{2\pi(z + 2f)}{\lambda} - j \frac{2\pi}{\lambda f} \times (x_s x + y_s y) - j \frac{\pi z}{\lambda f^2} (x_s^2 + y_s^2) \right], \quad (1)$$

where λ is the wavelength of light, f is the focal length of lens L1, and (x, y, z) are the coordinates behind lens L1 with their origin at the rear focal point of lens L1. Field $u(x, y, L)$ at object mirror M1 and field $u(x, y, L + 2\Delta z)$ at the corresponding location in the other arm of the interferometer are imaged and superposed to form interference fringes on the CCD image sensor. Note that the beam reflected from reference mirror M2 travels a distance $2\Delta z$ more than the object beam. Because each point source is completely incoherent to any other points on the source, the overall intensity on the image sensor contributed by all the source points is a sum of fringe intensities obtained from all the point sources:

$$I(x, y, L) = \iint \left| \frac{u_s(x_s, y_s)}{j\lambda f} \exp\left[j \frac{2\pi(L + 2f)}{\lambda} - j \frac{2\pi}{\lambda f} (x_s x + y_s y) - j \frac{\pi L}{\lambda f^2} (x_s^2 + y_s^2) \right] + \frac{u_s(x_s, y_s)}{j\lambda f} \exp\left[j \frac{2\pi(L + 2\Delta z + 2f)}{\lambda} - j \frac{2\pi}{\lambda f} (x_s x + y_s y) - j \frac{\pi(L + 2\Delta z)}{\lambda f^2} \times (x_s^2 + y_s^2) \right] \right|^2 dx_s dy_s, \quad (2)$$

where the integration is performed over the area of the extend source. After some straightforward algebra, the intensity distribution given by Eq. (2) becomes

$$I(x, y, L) = B\left\{ 1 + |\mu(2\Delta z)| \cos\left[-\frac{4\pi\Delta z}{\lambda} + \phi(2\Delta z) \right] \right\}, \quad (3)$$

where $B = (2/\lambda^2 f^2) \iint I_s(x_s, y_s)\mathrm{d}x_s\mathrm{d}y_s$. The function $\mu(\Delta z) = |\mu|\exp(j\phi)$ is the longitudinal complex degree of coherence given by

$$\mu(2\Delta z) = \frac{\iint I_s(x_s, y_s)\exp\left[j\,\frac{2\pi\Delta z}{\lambda f^2}\,(x_s^2 + y_s^2)\right]\mathrm{d}x_s\mathrm{d}y_s}{\iint I_s(x_s, y_s)\mathrm{d}x_s\mathrm{d}y_s}. \tag{4}$$

The analogy to diffraction theory will help our intuitive understanding of the principle. Let us consider diffraction from an aperture $u(x_s, y_s)$ in the source plane. From Eq. (1), the diffracted field in the plane at distance Δz_0 in front of the rear focal plane of lens L1 is given by

$$u(x, y, -\Delta z_0) = \frac{\exp[jk(2f - \Delta z_0)]}{j\lambda f}\iint u_s(x_s, y_s) \times \exp\left[-\frac{j2\pi}{\lambda f}\,(x_s x + y_s y) + \frac{j\pi\Delta z_0}{\lambda f^2}\,(x_s^2 + y_s^2)\right]\mathrm{d}x_s\mathrm{d}y_s. \tag{5}$$

If we put $2\Delta z = \Delta z_0$, we note that Eq. (4) is (apart from a constant factor) equivalent to axial field $u(0, 0, -\Delta z_0)$ created at distance Δz_0 in front of the rear focal plane of spherical lens L1:

$$u(0, 0, -\Delta z_0) = \frac{\exp[jk(2f - \Delta z_0)]}{j\lambda f}\iint u_s(x_s, y_s) \times \exp\left[\frac{j\pi\Delta z_0}{\lambda f^2}\,(x_s^2 + y_s^2)\right]\mathrm{d}x_s\mathrm{d}y_s. \tag{6}$$

From this analogy to the diffraction theory, our problem of producing high coherence for optical path difference $2\Delta z$ can be reduced to the problem of finding a real and nonnegative aperture distribution that produces a strong optical field on the optical axis at distance $2\Delta z$ from the rear focal point. Obviously a circular aperture whose transmittance has the form of a Fresnel zone plate can satisfy the above requirement if we chose

$$I_s(r_s) = (1/2)[1 + \cos(2\pi\gamma r_s^2 + \beta)], \tag{7}$$

where $r_s^2 = x_s^2 + y_s^2$ and β is the initial phase of the zone plate. A zone plate illuminated by a plane wave focuses light on the axis at distances $\Delta z_0 = 0, \pm 2\gamma\lambda f^2$ from the rear focal point. Correspondingly, a spatially incoherent source whose irradiance distribution has the same form as Eq. (7) produces fields that exhibit high coherence for the three optical path differences $2\Delta z = \pm 2\lambda f^2\gamma$ and $\Delta z = 0$. By modulating the source distribution with a spatial light modulator (SLM) and changing zone plate parameter γ monotonically, we scan the coherence function along the Δz axis. When a high-visibility peak is observed for some value γ_0 on the curve of visibility versus γ, it is a clear indication that object mirror M1 is located at a distance $\Delta z = \lambda f^2\gamma_0$ from reference mirror M2. Thus by means of the SLM we can control longitudinal spatial coherence without using mechanical moving components. If we assume a circularly symmetric source and introduce a new radial parameter $\rho_s = r_s^2 = x_s^2 + y_s^2$, we can express Eq. (4) in a simple form of the Fourier transform:

$$\mu(\Delta z) = \frac{\int_0^{R^2} I_s(\rho_s)\exp\left(j\,\frac{2\pi\Delta z\rho_s}{\lambda f^2}\right)\mathrm{d}\rho_s}{\int_0^{R^2} I_s(\rho_s)\mathrm{d}\rho}, \tag{8}$$

where R is the radius of circular source $I_s(\rho_s)$. As Eq. (7) becomes a sinusoid for variable ρ_s:

$$I_s(\rho_s) = [1 + \cos(2\pi\gamma\rho_s + \beta)]/2, \tag{9}$$

we have

$$\mu(\Delta z) \propto \left[\exp\left(\frac{j\pi R^2\Delta z}{\lambda f^2}\right)\mathrm{sinc}\left(\frac{\pi R^2\Delta z}{\lambda f^2}\right)\right] * [2\delta(\Delta z) + \exp(j\beta)\delta(\Delta z + \gamma\lambda f^2) + \exp(-j\beta)\delta(\Delta z - \gamma\lambda f^2)], \tag{10}$$

where $\mathrm{sinc}(x) = \sin(x)/x$, $\delta(x)$ is the Dirac delta function, and $*$ denotes convolution. Relation (10) gives three correlation peaks, and we can control the distance between the central and the side peaks by changing parameter γ of the zone plate with a SLM.

B. New Interpretation of Longitudinal Coherence Control Based on Haidinger Fringes of Equal Inclination

In this section we give a new interpretation of the principle of longitudinal coherence control in which the underlying physics for the coherence control is explained in terms of Haidinger fringes[16] of equal inclination. This new interpretation helps our intuitive understanding of the reason why the zone-platelike spatially incoherent source generates high-coherence fields for particular mirror distances Δz. In addition, it provides an insight into the practical problem of how to design the specific shape of the zone plate when the optical system has aberrations and misalignments.

As shown in Fig. 1, beam splitter BS forms a virtual image of reference mirror M2 at distance Δz behind object mirror M1, which serves as an effective reference mirror, M2′. The two mirrors M1 and M2′ together work as a plane-parallel plate with optical thickness Δz. If the plane-parallel plate is illuminated with an extended quasi-monochromatic spatially incoherent source, a set of Haidinger fringes of equal inclination (that is, localized at infinity) will be observed in the focal plane of lens L, as shown in Fig. 2. A ray from the source that is incident upon the

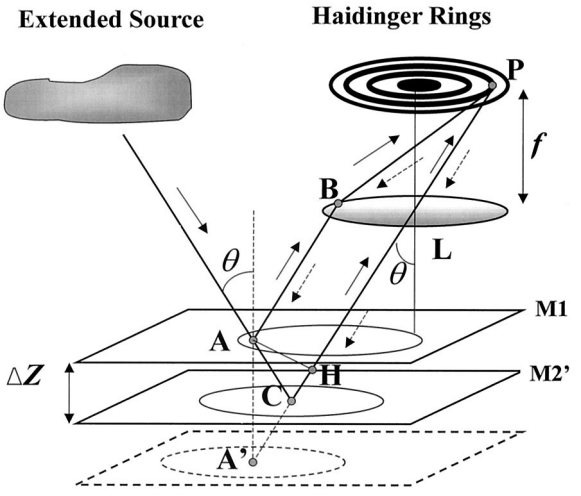

Fig. 2. Generation of Heiginger fringes of equal inclination and the inverse process of beam propagation.

plane-parallel plate at a small angle θ is reflected by the upper and lower surfaces, M1 and M2′, to form parallel rays *ABP* and *ACP*. The optical path difference between these two rays is given by

$$\begin{aligned}\overline{ACH} = \overline{A'H} &= 2\Delta z \cos\theta \\ &\approx 2\Delta z\left(1 - \frac{\theta^2}{2}\right) \\ &\approx 2\Delta z\left(1 - \frac{r^2}{2f^2}\right),\end{aligned} \tag{11}$$

where r is the radial distance of observation point P from the optical axis of lens L, f is the focal length of the lens, *AH* is a normal from point A to ray *CLP*, and A′ is a mirror image of point A with respect to plane M2′. Thus the normalized intensity of the Haidinger fringes observed at point P is given by

$$I(r) = \left(\frac{1}{2}\right)\left[1 + \cos\left(\frac{2\pi\Delta z}{\lambda f^2}\, r^2 - \frac{4\pi\Delta z}{\lambda}\right)\right]. \tag{12}$$

If we put $\gamma = \Delta z/\lambda f^2$ and $\beta = -4\pi\Delta z/\lambda$, we find that Eq. (12) has the same form as the Fresnel zone plate given by Eq. (6).

Let us now consider an inverse process in which lens L is illuminated from behind by a point source at P on the observation plane. On reflection from the lower surface, ray *PCA* meets ray *PBA* at point A, and the two rays interfere. When point source P lies on the bright fringes of the Haidinger rings, the interference at point A is constructive because optical path difference $\overline{ACH}$ is an integer multiple of wavelength λ. Similarly, the interference becomes destructive if the point source is on the dark fringes of the Haidinger rings. If lens L is illuminated with an extended quasi-monochromatic spatially incoherent source whose irradiance distribution is proportional to the intensity of the Haidinger fringes [given by Eq. (12)], only the point sources located on the bright fringes will participate in the interference. This means that, for every point source, interference occurs constructively, and uniform bright fringes are produced over upper plane M1. Because the source is spatially incoherent, the bright fringes produced by the individual point sources are superposed on an intensity basis. This in-phase superposition of many fringe intensities creates a spatially uniform bright fringe that is strongly localized on upper plane M1. Inasmuch as Eq. (12) does not change if Δz is replaced by $-\Delta z$, the same phenomenon will be observed when plane M1 is located at a distance $-\Delta z$ below plane M2′. When $\Delta z = 0$, ray PBA overlaps ray PHC, and constructive interference occurs irrespective of the position of point source P, because the optical path difference is zero.

So far, for ease of understanding, we have used the virtual optical system shown in Fig. 2, which includes virtual rays and a virtual mirror image of M2 formed by beam splitter BS. Based on this virtual optical system, our description included real fringes generated on upper mirror plane M1. In the actual optical system shown in Fig. 1, however, the fringes observed on mirror plane M1 through the beam splitter from the side of the CCD are virtual (rather than real) fringes. Therefore we need a lens, L2, that images mirror plane M1 onto the CCD image sensor and converts the virtual fringes into real fringes to be detected by the CCD sensor. Thus, referring to Fig. 1, extended incoherent source S, whose shape corresponds to the bright fringes of the Haidinger rings, produces an optical field that has a longitudinal coherence function with three peaks, which are observed when the distance between mirrors M1 and M2′ is 0 or $\pm\Delta z$.

The interpretation given above permits one to determine the specific shape and the location of the source for an imperfect optical system that has aberrations and misalignments. When the optical system has aberrations, the source with the shape of a circular zone plate given by Eq. (6) is no longer the best choice because the Haidinger fringes do not have a perfect circular shape. Generally, we do not know what kinds of aberration are present and how they influence the optimum shape of the source. Even if the system is free from aberration, it is generally not easy to find the exact location of the optical axis of the system to which the center of the zone-platelike source should be adjusted. Based on the new interpretation, we propose the following technique: Referring to Fig. 1, we first illuminate the interferometer with another extended quasi-monochromatic source inversely from the side of imaging lens L2 and the CCD camera; then we record the Haidinger fringes generated on plane S upon which the designed source is to be placed. Then we use the recorded intensity distribution of the Haidinger fringes as irradiance distribution $I_s(x_s, y_s)$ of the source to be placed upon S. When we illuminate the interferometer with this source distribution $I_s(x_s, y_s)$ through lens L1, we can generate an optical field that gives a high coherence peak for mirror distance Δz for

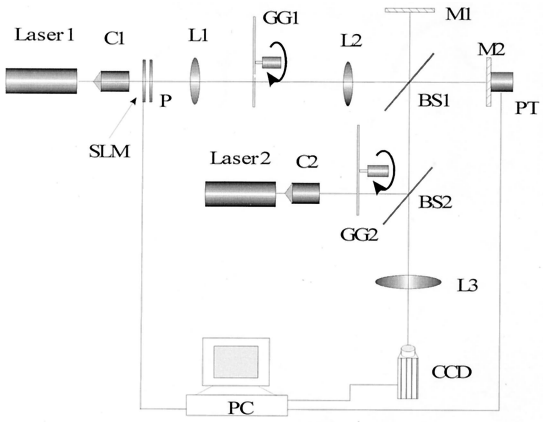

Fig. 3. Schematic illustration of the experimental system: C1, C2, collimator lenses; GG1, GG2, ground glass; transducer; BS1, BS2, beam splitters; other abbreviations defined in text.

which the Haidinger fringes were recorded. If we record a set of the Haidinger fringes and generate the corresponding source distributions with a SLM, we can perform tomographic imaging at the desired mirror distances determined by the longitudinal spatial coherence function synthesized by the SLM.

3. Experiments

Experiments have been conducted to demonstrate the validity of the principle. A schematic illustration of the experimental system is shown in Fig. 3. A Michelson interferometer is illuminated by two quasi-monochromatic spatially incoherent light sources; one is an extended source created by the beam from Laser2 to generate Haidinger fringes on ground glass GG1; the other serves as a source for spatial coherence synthesis. The two light sources are both He–Ne lasers with wavelength $\lambda = 0.6328$ μm. The beam from Laser1 was collimated by collimator C1 to illuminate a liquid-crystal SLM on which the Haidinger-fringe-like source irradiance distribution is displayed by a personal computer, PC. The source irradiance distribution displayed on the SLM is imaged by lens L1 onto rotating ground-glass plate GG1 to make a spatially incoherent source with the desired irradiance distribution. The light from each point on the ground glass is collimated by lens L2 and is introduced into a Michelson interferometer. One mirror, M1, was attached on a fixed arm to serve as an object mirror, and the other mirror, M2, served as a reference mirror. Mirror M2 was mounted upon a piezoelectric transducer, PT, for phase shift, and the piezoelectric transducer itself was placed upon a precision mechanical stage to form a variable arm. The two reflected beams from M1 and M2 were combined by beam splitter BS1 and passed by lens L3. Lens L3 forms an image of mirror M1 onto the CCD plane such that intensity of the fringes virtually localized on mirror M1 is recorded. According the principle described, the zone-plate-like distribution was generated by the personal computer and displayed on the SLM. The focal length of lens L2 was

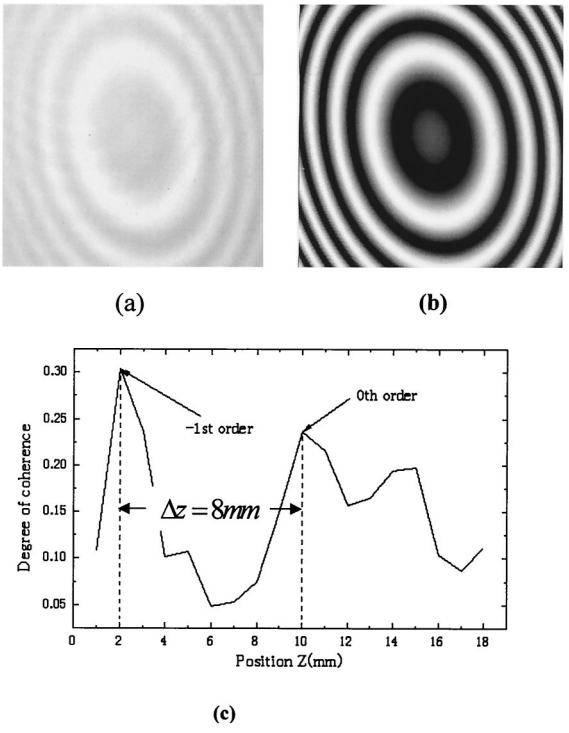

Fig. 4. (a) Haidinger fringes recorded for $\Delta z = 8$ mm. (b) Source irradiance distribution designed to have the same shape as the Haidinger fringes. (c) Longitudinal degree of coherence.

$f = 300$ mm. The experiments were performed as follows: First we turned on Laser2 only, and we observed the Haidinger fringes on ground glass GG1 by adjusting mirrors M1 and M2 to be exactly parallel. Subsequently, we produced a zone-plate-like pattern with the computer according to the Haidinger fringes that appear on GG1 and displayed the zone-plate-like pattern on the SLM. In this way we made the designed zone plate and Haidinger fringes match as closely as possible. Then, turning off Laser2 and switching on Laser1, we observed fringes virtually localized on mirror M1 through the CCD camera with lens L3 focused on M1. The fringes have uniform illumination over the field of view because M1 and M2 have been made parallel, and they are high contrast because the source shape is tuned to the Haidinger fringes generated at the present mirror position. By moving the position of mirror M2 we changed the optical path difference between the two arms of the Michelson interferometer and measured the visibility of the fringes by a phase-shift technique.[17] In this way we obtained the distribution of degree of coherence along the axis.

Figure 4(a) shows an example of Haidinger fringes recorded by a CCD camera placed at the position of ground glass GG1. Because of the astigmatism introduced by the optical system, the Haidinger fringes have the shape of an ellipse, which can be modeled by the following formula:

$$I(x_s, y_s) \propto 1 + \cos\{2\pi[\gamma(x_s^2 + y_s^2) + A_0(x_s^2 - y_s^2) + B_0 x_s y_s] + \beta\}, \quad (13)$$

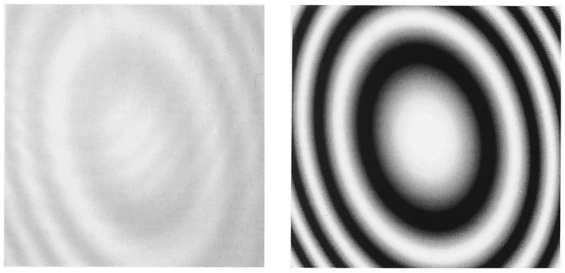

(a) (b)

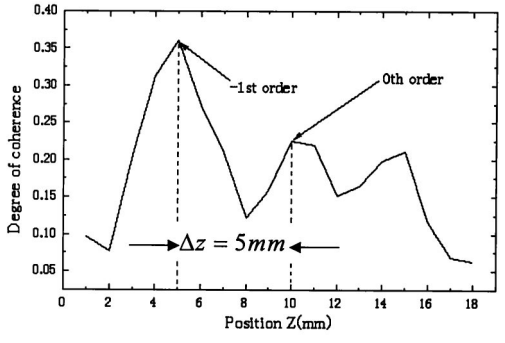

(c)

Fig. 5. (a) Haidinger fringes recorded for $\Delta z = 5$ mm. (b) Source irradiance distribution designed to have the same shape as the Haidinger fringes. (c) Longitudinal degree of coherence. Optical path difference, zero; $\Delta z = 0$ at position $z = 10$ mm on the horizontal axis.

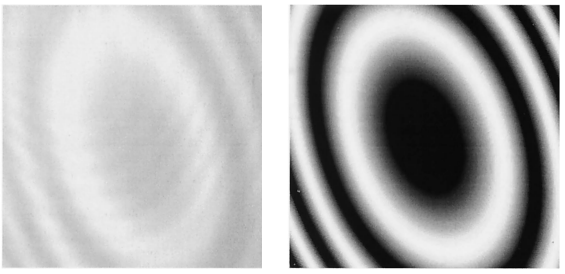

(a) (b)

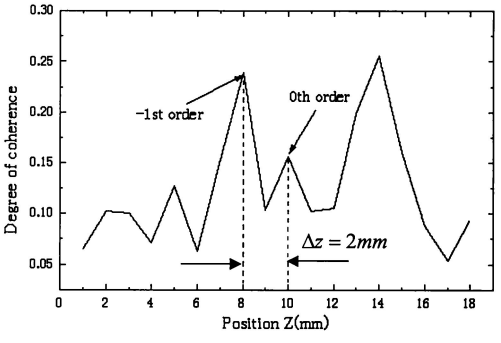

(c)

Fig. 6. (a) Haidinger fringes recorded for $\Delta z = 2$ mm. (b) Source irradiance distribution designed to have the same shape as the Haidinger fringes. (c) Longitudinal degree of coherence. Optical path difference, zero; $\Delta z = 0$ at position $z = 10$ mm on the horizontal axis.

where A_0 and B_0 parameterize the astigmatism and parameters γ and β correspond to those of an ideal zone plate in Eq. (7). If we remember that Eq. (7) gives $\gamma = \Delta z/\lambda f^2$ in the aberration-free case, we can expect from formula (13) that, as we reduce the mirror distance, the elliptic fringe pattern will change its shape and become a hyperbola for $\Delta z = 0$. If we move the mirror farther beyond to the region of $-\Delta z$, the fringe pattern will become elliptical again but with the ellipses' major and minor axes interchanged. This is indeed what we observed experimentally. From this phenomenon we identified the location of $\Delta z = 0$ to be at 10 mm of the dial reading of the stage. Note that, just as the temporally incoherent white-light source does, a quasi-monochromatic spatially incoherent source provides information about the location of $\Delta z = 0$. The Haidinger fringes shown in Fig. 4(a) are recorded for $\Delta z = 8$ mm (which corresponds to the stage dial reading of 2 mm). Figure 4(b) shows the irradiance distribution of the source designed by computer, which has the same shape as the Haidinger fringes in Fig. 4(a). Moving the stage in 1-mm steps, we measured the coherence function (the fringe contrast) by using the phase-shift technique.[17] The result is shown in Fig. 4(c). As designed, a coherence peak is observed at the position of 2 mm in the stage dial reading that corresponds to $\Delta z = 8$ mm. The peak for $\Delta z = 0$ is also observed at the correct position, 10 mm in the stage dial reading, but the peak height is lower than that for $\Delta z = 8$ mm. The peak for $\Delta z = -8$ mm is not clearly observed. This can be explained by the degree of overlap of the source shape (or the shape of the Haidinger fringes) for $\Delta z = 8$ mm with those for $\Delta z = 0$ and $\Delta z = -8$ mm. We can observe the lower peak for $\Delta z = 0$ because the ellipse for $\Delta z = 8$ mm has some overlap with the hyperbola for $\Delta z = 0$. However, the ellipse for $\Delta z = 8$ mm has much less overlap with the ellipse for $\Delta z = -8$ mm because the major and minor axes of these ellipses are interchanged. Figure 5(a) shows the Haidinger fringes for $\Delta z = 5$ mm, and Fig. 5(b) is the corresponding source irradiance distribution. As shown in Fig. 5(c), a coherence peak is observed at position 5 mm, which corresponds to $\Delta z = 5$ mm. Similarly, the Haidinger fringes for $\Delta z = 2$ mm and the corresponding source irradiance distribution are shown in Figs. 6(a) and 6(b), respectively. Here again we observe a coherence peak at position 8 mm, which corresponds to $\Delta z = 2$ mm. The relationship between parameter γ and mirror distance Δz for the coherence peak was plotted as shown in Fig. 7. With the change of parameter γ, other parameters, A_0 and B_0, were changed by the same factor. Because of astigmatism, Δz is not exactly proportional to parameter γ, but Δz increases linearly with γ. This means that even for an optical system with astigmatism, the position of the coherence peak can be controlled by the spatial frequency of the zone plate.

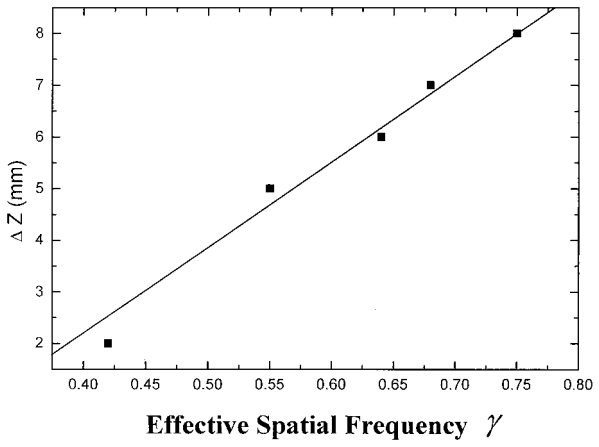

Fig. 7. Relationship between the optical path difference for the first coherence peak and effective spatial frequency.

4. Discussion

We briefly discuss some of the factors that affect the performance of the proposed technique. First, we focus on the influence of the tilt introduced between the two mirrors of the Michelson interferometer and show that the tilt produces a crucial effect. Then we discuss other alignment issues and clarify the reason why we use the second laser to generate Haidinger fringes.

A. Influence of Tilts

Let us note again the collimated beam from point source A at point (x_s, y_s) on the incoherent source in stituting $x_s \rightarrow (x_s - \alpha_x)$ and $y_s \rightarrow (y_s - \alpha_y)$ for the beam from mirror M1, we have from Eq. (2)

$$I(x, y, L) = \iint \left| \frac{u_s(x_s, y_s)}{j\lambda f} \exp\left[j \frac{2\pi(L + 2f)}{\lambda} - j \frac{2\pi}{\lambda f}(x_s x + y_s y) - j \frac{\pi L}{\lambda f^2}(x_s^2 + y_s^2) \right] + \frac{u_s(x_s, y_s)}{j\lambda f} \exp\left\{ j \frac{2\pi(L + 2\Delta z + 2f)}{\lambda} - j\frac{2\pi}{\lambda f}[(x_s - \alpha_x)x + (y_s - \alpha_y)y] - j \frac{\pi(L + 2\Delta z)}{\lambda f^2}[(x_s - \alpha_x)^2 + (y_s - \alpha_y)^2] \right\} \right|^2 \mathrm{d}x_s \mathrm{d}y_s. \quad (14)$$

We have

$$I(x, y, L) = A\left\{ 1 + |\mu(2\Delta z)| \cos\left[-\frac{4\pi\Delta z}{\lambda} + \phi(2\Delta z) - \frac{2\pi}{\lambda f}(\alpha_x x + \alpha_y y) + \frac{\pi(L + 2\Delta z)}{\lambda f^2}(\alpha_x^2 + \alpha_y^2) \right] \right\}, \quad (15)$$

which corresponds to Eq. (3) and where the longitudinal complex degree of coherence is now given by

$$\mu(\alpha_x, \alpha_y, 2\Delta z) = \frac{\iint I_s(x_s, y_s) \exp\left[\frac{j2\pi\Delta z}{\lambda f^2}(x_s^2 + y_s^2) - \frac{j2\pi(L + 2\Delta z)}{\lambda f^2}(x_s\alpha_x + y_s\alpha_y) \right] \mathrm{d}x_s \mathrm{d}y_s}{\iint I_s(x_s, y_s) \mathrm{d}x_s \mathrm{d}y_s}. \quad (16)$$

Fig. 1. When object mirror M1 is tilted by a small angle (θ_x, θ_y), the direction of the reflected beam deviates by an angle $(2\theta_x, 2\theta_y)$ from its original direction. Observed from the side of L2 and CCD through beam splitter BS, this introduction of angular deviation is equivalent to giving lateral displacement $(\alpha_x, \alpha_y) = (f \sin 2\theta_x, f \sin 2\theta_y)$ to the point source. Subtion. Observed from the side of L2 and CCD through beam splitter BS, this introduction of angular deviation is equivalent to giving lateral displacement $(\alpha_x, \alpha_y) = (f \sin 2\theta_x, f \sin 2\theta_y)$ to the point source. Sub-

Equation (16) has a form similar to that of the three-dimensional complex degree of coherence derived from the generalized van Cittert–Zernike theorem[12]:

$$\mu(\Delta x, \Delta y, 2\Delta z) = \frac{\iint I_s(x_s, y_s) \exp\left[\frac{j2\pi\Delta z}{\lambda f^2}(x_s^2 + y_s^2) - \frac{j2\pi}{\lambda f}(x_s\Delta x + y_s\Delta y) \right] \mathrm{d}x_s \mathrm{d}y_s}{\iint I_s(x_s, y_s) \mathrm{d}x_s \mathrm{d}y_s}. \quad (17)$$

Apart from scale factor $(L + 2\Delta z)/f$, the tilt gives the same effect as lateral coherence in the three-dimensional complex degree of coherence. Note also the similarity of Eq. (16) to Eq. (5), which gives a

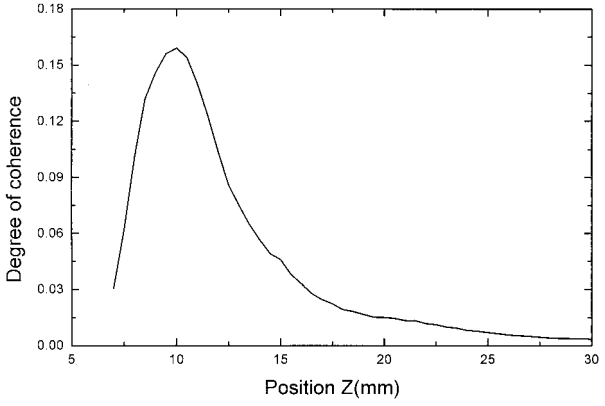

Fig. 8. Longitudinal degree of coherence when a small tilt angle was introduced. The contrast peak at $z = 10$ mm corresponds the position of $\Delta z = 0$.

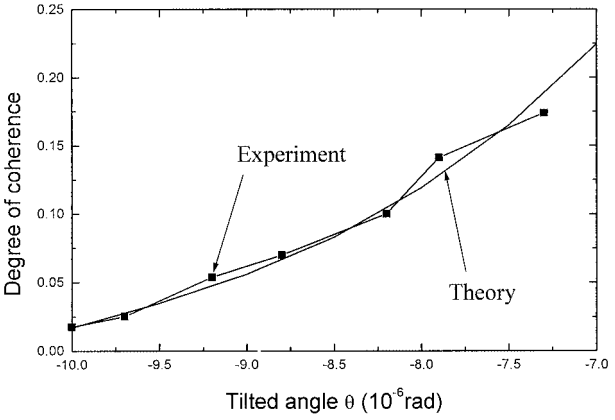

Fig. 9. Relationship between degree of coherence and tilt angle.

diffraction field about the focal point. Generally, a point-spread function of an imaging system has a far smaller spread in the lateral direction than in the longitudinal direction. Analogously, lateral coherence decreases far more quickly than longitudinal coherence. To see the effect of tilt, we put $\Delta z = 0$ into Eq. (16) and assume a uniform circular source of radius R. Adopting polar coordinate systems ($\alpha_x = \alpha \cos \xi$, $\alpha_y = \alpha \sin \xi$) and ($x_s = r_s \cos \eta$, $y_s = r_s \sin \eta$), we have from Eq. (16)

$$\mu(0) = \frac{\int_0^{2\pi} \int_0^R I_s(r_s) \exp\left[-j \frac{2\pi L}{\lambda f^2} \alpha r_s \cos(\xi - \eta) \right] r_s \mathrm{d}r_s \mathrm{d}\eta}{\int_0^{2\pi} \int_0^R I_s(r_s) r_s \mathrm{d}r_s \mathrm{d}\eta} = \frac{2J_1(2\pi LR\alpha/\lambda f^2)}{2\pi LR\alpha/\lambda f^2} = \frac{2J_1(4\pi LR\theta/\lambda f)}{4\pi LR\theta/\lambda f}, \quad (18)$$

where J_1 is the first-order Bessel function and θ is a tilt angle approximated by $2\theta \approx \alpha/f$. Even for an aberration-free system with $\Delta z = 0$, fringe contrast is reduced significantly by the introduction of a small amount of tilt. Specifically, for $L = 100$ mm, $R = 5$ mm, $\lambda = 630$ nm, and $f = 150$ mm, a small tilt angle of 5.8×10^{-5} rad makes the fringe contrast zero. An example of the experimental observation of a coherence function for a tilted mirror is shown in Fig. 8. Only the 0th peak (for which $\Delta z = 0$) was observed, with very low contrast. Although we used a zone-platelike source, the first peak (for which $\Delta z = \lambda f^2 \gamma_0$) disappeared. A variation of fringe contrast with the amount of tilt was observed by experiment. In Fig. 9 the solid curve shows the degree of coherence predicted by the theory; the value of the curve is reduced monotonically with the tilted angle. The curve predicted by the theory was scaled appropriately to fit the experimental data, with its Bessel sinc function form preserved. The fringe contrasts were measured by Fourier fringe analysis.[18] Because Fourier fringe analysis requires the interferogram to have at least several fringes that serve as a spatial carrier frequency for signal separation in the spatial-frequency domain, we were not able to measure the degree of coherence for very small tilt angles (close to zero). Despite the restricted range of measurement, the curves indicate reasonable agreement between the experimental data and the theoretical prediction.

For an ideal case without tilt and aberrations, it is obvious from Schwartz's inequality that the modulus of the longitudinal complex degree of coherence given by Eq. (4) takes a maximum value of unity for $\Delta z = 0$. When tilt is present, as can be seen from Eq. (16), the modulus of the longitudinal complex degree of coherence does not necessarily takes a maximum value for $\Delta z = 0$, and the location of the maximum coherence depends on the tilt and the aberrations introduced.

In the application of the proposed technique to optical tomography and profilometry, the first coherence peak (for which $\Delta z = \lambda f^2 \gamma_0$) serves as an indicator for the location of the test surface. If the first contrast peak disappears because of tilts, we cannot obtain any information about the distance between the test surface and the reference mirror. One may therefore regard this high sensitivity to tilts as a fundamental drawback of the proposed method. However, if one looks at the matter from another viewpoint, one may find that the characteristic of high sensitivity to tilts can be a great advantage. We now have an unconventional interferometric system with the unique characteristic that high-contrast fringes are created only at locations where both the surface height and the local surface inclination satisfy the particular conditions set by the structure of

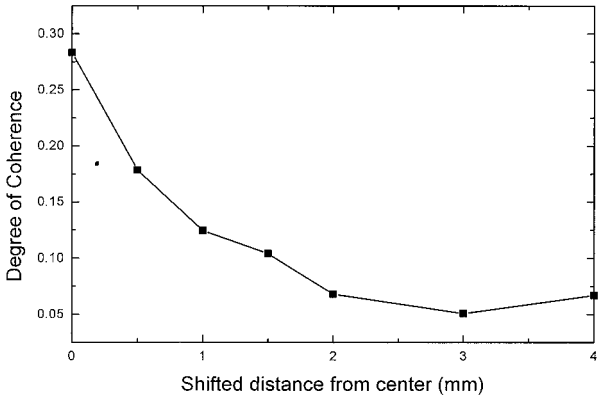

Fig. 10. Relationship between degree of coherence and decentering.

the zone-plate-like source and the orientation of the reference mirror. This characteristic can be exploited, for example, for simultaneous detection of the distance and the local surface inclination of an object, which remains a subject for future research.

B. Influence of Source Misalignments

For the proposed principle to work, the center of the zone-plate-like source must be precisely adjusted to the axis of the optical system. For an actual optical system, it is a difficult to find the exact location of the optical axis. Besides the effect of tilts, the phenomenon that the first order is greater than the zero order can occur if the center of the zone plate is not on the optical axis. In this case the line connecting zero and the first order is not parallel to the axis $(\alpha_x, \alpha_y) = (0, 0)$. The analogous case to this phenomenon from diffraction theory can be found in Ref. 19. Thus the tilt and the effect of the noncentered zone-plate-like source together can explain the phenomenon that the first order is a peak above all the rest, which we observed in our experiments.

We experimentally examined the influence of source decentering on the degree of coherence. As shown in Fig. 10, fringe contrast is reduced significantly as the amount of decentering increases. The new interpretation of the principle in relation to Haidinger fringes gives a solution to this source-misalignment problem. As explained in Subsection 4.A, Haidinger fringes generated by the second laser provide information about where the zone plate should be placed and what of the zone-plate shape should be adopted to create high longitudinal coherence at the desired optical path distance.

5. Conclusions

We have proposed a new method for controlling the longitudinal degree of coherence that has the potential application in tomography by use of a spatial light modulator to change the source intensity distribution. Unlike conventional techniques used for the measurement of surface profiles, the proposed technique permits tomographic measurement without changing the optical path difference between the two arms of the interferometer. The proposed interferometric system has the unique characteristic that high-contrast fringes are created only at locations where both the surface height and the local surface inclination satisfy the specific conditions set by the structure of the zone-plate-like source and the orientation of the reference mirror. This characteristic has a potential application to the simultaneous detection of the distance and the local surface inclination of an object. We have discussed the performance of the proposed technique with particular focus on alignment issues, including the influence of tilts and source decentering. We have presented a new interpretation of the principle and proposed a treatment of source-alignment issues based on the new interpretation.

This research was performed when Wei Wang was a visiting graduate student at the University of Electro-Communication under the program of Japanese University Studies in Science and Technology, supported by the Association of International Education, Japan. Part of this research was supported by grant-in-aid 13450029 from the Ministry of Education, Science, Culture and Sports of Japan.

We express our cordial thanks to Alexander V. Tavrov and Dalip Singh Mehta for helpful discussions. We also wish to thank Shuuji Hattori for his help with the computer hardware.

References

1. R. C. Youngquist, S. Carr, and D. E. N. Davies, "Optical coherence-domain reflectometry: a new optical evaluation technique," Opt. Lett. **12,** 158–160 (1987).
2. D. Huang, E. A. Swanson, C. P. Lin, J. S. Schuman, W. G. Stinson, W. Chang, M. R. Hee, T. Flotte, K. Gregory, C. A. Puliafito, and J. G. Fujimoto, "Optical coherence tomography," Science **254,** 1178–1181 (1991).
3. X. J. Wang, T. E. Milner, J. F. de Boer, Y. Zhang, D. H. Pashley, and J. S. Nelson, "Characterization of dentin and enamel by use of optical coherence tomography," Appl. Opt. **38,** 2092–2096 (1999).
4. P. A. Flournoy, R. W. McClure, and G. Wyntjes, "White-light interferometric thickness gauge," Appl. Opt. **11,** 1907–1915 (1972).
5. M. Davidson, K. Kaufman, I. Mazor, and F. Cohen, "An application of interference microscopy to integrated circuit inspection and metrology," in *Integrated Circuit Metrology, Inspection, & Process Control*, K. M. Monahan, ed., Proc. SPIE **775,** 233–247 (1987).
6. B. S. Lee and T. C. Strand, "Profilometry with a coherence scanning microscope," Appl. Opt. **29,** 3784–3788 (1990).
7. T. Dresel, G. Hausler, and H. Venzke, "Three-dimensional sensing of rough surfaces by coherence radar," Appl. Opt. **31,** 919–925 (1992).
8. L. Mandel and E. Wolf, *Optical Coherence and Quantum Optics*, 1st ed. (Cambridge U. Press, Cambridge, 1995), Chap. 4, p. 149.
9. M. Takeda, "The philosophy of fringes—analogies and dualities in optical metrology," in *Fringe '97*, *Proceedings of the Third International Workshop on Automatic Processing of Fringe Patterns*, W. Jueptner and W. Osten, eds. (Akademie-Verlag, Berlin, 1997), pp. 17–26.
10. C. W. McCutchen, "Generalized source and the Van Cittert–

Zernike theorem: a study of the spatial coherence required for interferometry," J. Opt. Soc. Am. **56,** 727–733 (1966).
11. J. E. Biegen, "Determination of the phase change on reflection from two-beam interference," Opt. Lett. **19,** 1690–1692 (1994).
12. J. Rosen and A. Yariv, "General theorem of spatial coherence: application to three-dimensional imaging," J. Opt. Soc. Am. A **13,** 2091–2095 (1996).
13. J. Rosen and A. Yariv, "Longitudinal partial coherence of optical radiation," Opt. Commun. **117,** 8–12 (1995).
14. J. Rosen and M. Takeda, "Longitudinal spatial coherence applied for surface profilometry," Appl. Opt. **39,** 4107–4111 (2000).
15. K. Hotate and T. Okugawa, "Optical information-processing by synthesis of the coherence function," J. Lightwave Technol. **12,** 1247–1255 (1994).
16. F. A. Jenkins and H. E. White, *Fundamentals of Optics* (McGraw-Hill, New York, 1981), Chap. 14, p. 292.
17. J. H. Bruning, D. J. Herriott, J. E. Gallagher, D. P. Rosenfeld, A. D. White, and D. J. Brangaccio, "Digital wavefront measurement interferometer," Appl. Opt. **13,** 2693–2703 (1974).
18. M. Takeda, H. Ina, and S. Kobayashi, "Fourier-transform method of fringe-pattern analysis for computer-based topography and interferometry," J. Opt. Soc. Am. **72,** 156–160 (1982).
19. J. Rosen, B. Salik, and A. Yariv, "Pseudo-nondiffracting beams generated by radial harmonic functions," J. Opt. Soc. Am. A **12,** 2446–2457 (1995).